Grain consolidation and electrical conductivity in porous media

James N. Roberts and Lawrence M. Schwartz
Schlumberger-Doll Research, Old Quarry Road, Ridgefield, Connecticut 06877-4108
(Received 1 October 1984)

A simple geometrical model is proposed for diagenesis. Diagenesis is the process by which granular systems evolve geologically from unconsolidated, high-porosity packings toward more consolidated, less porous, materials. We find that the relation between the electrical conductivity σ and the porosity ϕ can be approximated by a nontrivial power law over a wide range of porosity for both *ordered* and *disordered* lattice configurations. The most realistic model is generated from a dense disordered packing. This leads to a problem involving both short-range structural disorder and correlated percolation. In comparison with experiment, our calculations (on both ordered and disordered systems) are shown to reproduce the qualitative trends found in recent data on the conductivity of systems comprised of fused glass beads.

I. INTRODUCTION

One of the most basic and useful empirical rules to emerge from the study of sedimentary materials is Archie's law,[1] which describes the electrical conductivity σ of a fluid-saturated system:

$$\sigma=\sigma_f\phi^m . \tag{1}$$

Here the porosity ϕ is the volume fraction of the pore-space network, σ_f is the fluid conductivity (the complementary grain space is insulating), and m is an exponent that depends on the characteristics of the system. Equation (1) should be viewed as a relation satisfied by a *family* of porous systems with a range of porosities and a *common geophysical history,* rather than as a constraint on the behavior of any one isolated material. (Indeed, for a single system, the only measurable quantities are σ and ϕ, and Eq. (1) reduces to the definition $m\equiv[\ln(\sigma)-\ln(\sigma_f)]/\ln(\phi)$.)

While it is obvious that σ should be directly proportional to σ_f, the intriguing aspects of Eq. (1) are that (1) the exponent m is noninteger, and (2) it predicts that a slight amount of conductivity persists down to zero porosity, rather than having σ vanish at a finite percolation threshold. While the second point has received considerable discussion,[2–5] in our opinion this feature of Archie's law must be interpreted with care. The electrical conductivity of very low porosity rocks ($\phi\lesssim 0.04$) is frequently controlled by *secondary porosity,* i.e., complexes of cracks and fractures that were not present in the original pore system.[6] Low-porosity systems with uniform evolutionary histories have been produced synthetically by sintering[7] and hot pressing,[8] and the connected paths in these systems have been observed to vanish when the porosity reaches 2–4 %.[8] (Materials that are cemented rather than compacted may well percolate at lower porosities, though this is difficult to test in a controlled environment.) Whether the conductivity threshold of sedimentary rocks occurs at precisely zero porosity or at a slightly higher value, there is no question that, as a class of disordered systems, they remain conducting down to much lower porosities than would be expected based on percolation-theory estimates.[9]

In the present paper a model is developed that can be used to represent granular systems with a wide range of porosities and a wide variety of ordered and disordered structures. In each case, the system initially consists of a tightly packed aggregate of hard spherical grains of uniform radius. As the system moves towards lower porosity, the grains are gradually distorted until, at the end of the process, they become a set of space-filling polyhedra. This evolution represents in a simple and reasonable way the diagenetic processes of cementation and compaction by which high-porosity granular sediments are transformed into less porous materials.[10–12] While our model does not remain conducting to the limit $\phi\rightarrow 0$ (the threshold is at $\phi\approx 0.03$), its attractive features are that (1) it is based on a realistic picture of the consolidation process by which sedimentary materials evolve toward lower porosities, (2) it shows how nontrivial power-law relations between σ and ϕ can be understood in terms of the way that different parts of the pore space are affected by consolidation, and (3) it makes clear that behavior consistent with Eq. (1) can be exhibited by both *ordered and disordered* systems.

Recent authors[2,3,5] have devoted considerable effort to the explanation of Archie's law. The common features of their work are, first, that they employ simplified models that treat either the grain or pore space (but not both) in a way that guarantees conductivity down to $\phi=0$ and, second, that they focus on the disorder inherent in most porous systems.[13] By contrast, we model the pore and grain spaces on an equal footing. The pore space is divided into relatively open regions (nodes) connected by relatively narrow regions (throats). Most of the porosity is concentrated in the nodes, while the throats dominate the electrical conductivity. We argue that Archie's law can be understood in terms of the natural evolution of these two segments of the pore space. Having said this, it should be emphasized that there are important links between our work and those of previous authors. This is particularly true in the case of Ref. 5, where a model based on a sim-

ple cubic array of tubes is used to study the electrical conductivity and permeability of porous media. The tube's diameters are reduced by a Monte Carlo algorithm to produce a skewed distribution of pore cross sections. Wong *et al.* emphasize that, for each ϕ, there are large tubes that control the mean porosity and smaller, more probable tubes that control the transport processes. Variations in the difference between these two measures of the pore space is shown to produce a power-law relation between σ and ϕ with an exponent m that depends on the degree of skewness in the pore-diameter distribution. From the earlier literature, perhaps the most relevant paper is Owen's work on electrical tortuosity[14] which applies a procedure similar to ours to a regular lattice of abstractly shaped pores and obtains behavior consistent with Eq. (1).

II. ORDERED CUBIC PACKINGS

To illustrate our ideas, let us begin with the simple example of spherical grains densely packed on a simple cubic (sc) lattice. The porosity of this system is $\phi=1-\pi/6\approx 0.48$. Keeping the lattice constant a fixed, we allow the grain radius to increase from its initial value of $R=1$ (see Fig. 1). In the region where the spheres overlap, the grains are truncated in such a way that the intergrain contacts evolve from points (for $R=1$) to circles on the faces of the Wigner-Seitz cell. Clearly, as R increases, the grains become nonspherical, and the porosity decreases. An elementary calculation yields the relation as follows

For sc, $1\le R\le\sqrt{2}$ $(a=2)$:

$$\phi(R)=1-\frac{\pi}{6}-\frac{\pi}{2}(R-1)+\frac{\pi}{4}(R-1)^2+\frac{\pi}{3}(R-1)^3 . \quad (2)$$

The geometry of this model remains relatively simple until $R=\sqrt{2}$, which corresponds to a porosity of 0.0349. At this point the contact circles touch the edges of the Wigner-Seitz cell and the pore space becomes disconnected. The system has reached a percolation threshold. Its pore space is divided into disjoint regions and the conductivity and permeability of the pore fluid vanish. What is interesting about this model is that its porosity spans a range of more than an order of magnitude between the original close-packed configuration (ϕ_{cp}) and the percolation limit (ϕ_c). Within this range the model retains the essential features of many granular porous systems: (1) the pore and grain spaces form interconnecting channels,[15] (2) individual grains are identifiable and are of comparable size,[16] and (3) the grains are joined at contacts that extend over a finite area. In Table I we show that similar results are obtained if this grain-growing algorithm is applied to sphere packs that are originally in body-centered-cubic (bcc) or face-centered-cubic (fcc) configurations. The equations corresponding to (2) for these systems are the following.

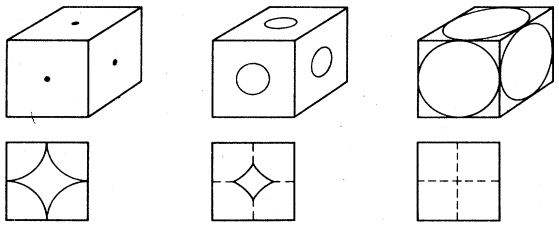

FIG. 1. (Upper) Wigner-Seitz cells for the simple cubic lattice at three stages of grain consolidation: The initial configuration of close-packed spheres, an intermediary stage, and the percolation threshold. The contacts are indicated on all of the visible cell faces but the grain within the cell is not shown. (Lower) Cross sections of the narrowest part of the throat at the same three stages of consolidation.

For bcc, $1\le R\le\sqrt{3/2}$ $(a=4/\sqrt{3})$:

$$\phi=1-\frac{\sqrt{3}\pi}{8}-\frac{3\sqrt{3}\pi}{8}(R-1)+\frac{3\sqrt{3}\pi}{8}(R-1)^2+\frac{3\sqrt{3}\pi}{8}(R-1)^3+\frac{3\pi}{8}\Theta(\sqrt{3}R-2)[(\sqrt{3}R-2)^2+\tfrac{1}{3}(\sqrt{3}R-2)^3] . \quad (3)$$

For fcc, $1\le R\le 2/\sqrt{3}$ $(a=2\sqrt{2})$:

$$\phi=1-\frac{\pi}{3\sqrt{2}}-\frac{\pi}{\sqrt{2}}(R-1)+\frac{2\pi}{\sqrt{2}}(R-1)^2+\frac{5\pi}{3\sqrt{2}}(R-1)^3 . \quad (4)$$

In Eq. (3), $\Theta(x)$ denotes the unit step function: $\Theta(x)=1$ for $x\ge 0$ and $\Theta(x)=0$ for $x<0$. In the fcc case, all the faces of the Wigner-Seitz cell are equivalent and the derivation of Eq. (4) is no more difficult than that of Eq. (2). By contrast, in the bcc case, the growing sphere first breaks through the hexagonal faces of the Wigner-Seitz cell and then, at $R=2/\sqrt{3}$, breaks through the square faces.

TABLE I. Porosity limits for the grain-consolidation model. (— indicates that a value is intentionally omitted.)

Initial distribution of grain centers	ϕ_{cp}	ϕ_c
Simple cubic	0.476	0.0349
Body-centered cubic	0.320	0.0055
Face-centered cubic	0.260	0.0359
Monte Carlo distribution[a]	—	0.032±0.004
Dense random packing	0.364	0.030±0.004[b]

[a]Reference 19.
[b]Reference 26.

Before considering the application of our model to more realistic initial arrangements, let us estimate, qualitatively, the behavior of the electrical resistivity. We can picture the conducting paths through the pore space as a series connection of low-resistance regions (the nodes) and high-resistance regions (the throats). The porosity dependence of the conductivity will then be dominated by the variation of the minimum cross-sectional area $A_{\min}$ of a typical throat (see Fig. 1). In the case of the simple cubic packing, for example, we find the following.

For sc :

$$\sigma \sim A_{\min} = 4 - \pi R^2 + (2R)^2 \times \sin^{-1}[(1-R^{-2})^{1/2}] - 4(R^2-1)^{1/2} . \tag{5}$$

The corresponding expressions for the body- and face-centered packings are the following.

For bcc :

$$\sigma \sim A_{\min} = \frac{4}{3\sqrt{2}} - \frac{\pi R^2}{4} + R^2 \sin^{-1}[(1-R^{-2})^{1/2}] - (R^2-1)^{1/2} + \tfrac{1}{2}\Theta(\sqrt{3}R-2) \times \left\{ R^2 \sin^{-1}\{[1-4/(3R^2)]^{1/2}\} - \frac{2}{\sqrt{3}}[R^2-(4/3)]^{1/2} \right\} . \tag{6}$$

For fcc :

$$\sigma \sim A_{\min} = \sqrt{3} - \frac{\pi R^2}{2} + 3R^2 \sin^{-1}[(1-R^{-2})^{1/2}] - 3(R^2-1)^{1/2} . \tag{7}$$

In Fig. 2 we plot this estimated resistivity versus the porosity for the three ordered lattice configurations. (The constant of proportionality between σ and $A_{\min}$ fixes the vertical position of the curve and is an adjustable parameter. Note, though, that the curve must pass through the origin [i.e., the point (1.0,1.0)] of Fig. 2 with a slope of 1.5 (see Ref. 2).) As ϕ decreases from ϕ_{cp}, all three curves exhibit behavior consistent with Eq. (1) over an appreciable concentration range. The values of m are approximately 1.80 for the simple cubic lattice, 1.35 for the body-centered cubic and 1.90 for the face-centered cubic. The slope of the body-centered system is noticeably lower than that of the simple or face-centered systems, which is consistent with this system having by far the lowest percolation threshold ($\phi_c = 0.0055$). At lower porosities, all three curves rise more rapidly as $\phi \to \phi_c$ and the throat cross sections are being closed off.

It may seem surprising that the relatively simple functions defined by Eqs. (5)—(7), when plotted against their counterparts in Eqs. (2)—(4) yield the curves shown in Fig. 2. To see what is happening let us consider the simple cubic case in more detail. Suppose we define the function $M(R)$ as follows:

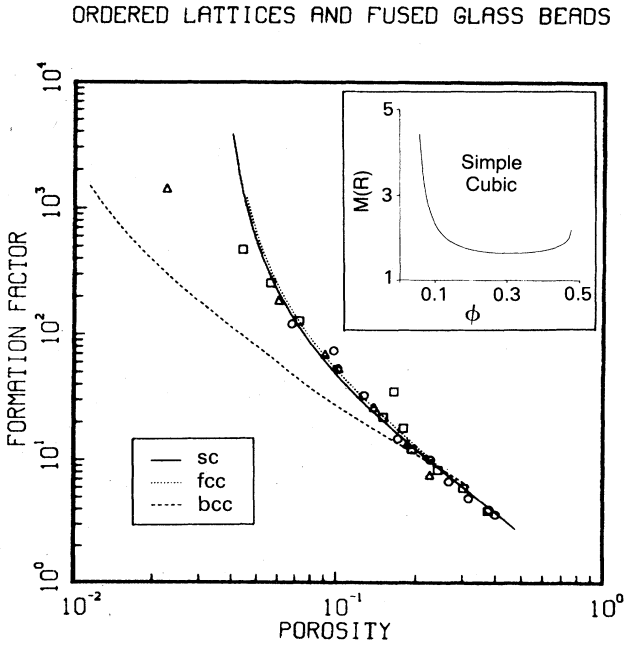

FIG. 2. Estimated formation factor (electrical resistivity) of the simple cubic (sc), face-centered cubic (fcc), and body-centered cubic (bcc) lattices. The vertical axis represents the ratio of the bulk resistivity to the fluid resistivity (σ_f/σ). A free scaling parameter in the computations was used to adjust the curves vertically to fit a set of measurements from fused glass beads. The circles, squares, and triangles represent measurements from three batches of beads with diameters in the ranges 44—53 μm (circles), 88—106 μm (squares), and 176—210 μm (triangles) (Ref. 5). (Inset) The behavior of $M(R)$ [Eq. (8)] is shown for a simple cubic lattice.

$$\frac{d\sigma/dR}{\sigma} \equiv M(R)\frac{d\phi/dR}{\phi} . \tag{8}$$

If $M(R)=m$ (a constant), then we would have true power-law behavior between σ and ϕ. In the present case, $M(R)$ is essentially (but not strictly) constant over a fairly wide range of porosities (see the inset in Fig. 2), and we have behavior that is a good approximation to a true power law within this range. [We emphasize that Archie's law is simply an *empirical* statement of the fact that rocks in a given family will satisfy Eq. (1) (approximately) over a given porosity range.]

Also shown in Fig. 2 are measured resistivities for a sequence of materials comprised of spherical glass beads that were sintered to obtain successively lower porosities.[5] Note that the experimental results also show a crossover to more rapid variation as the porosity is decreased below $\phi \approx 0.10$. The extremely high level of agreement between the experimental data and the present calculations for the simple and face-centered systems is, no doubt, fortuitous. Nevertheless, we believe that the model we have described captures an essential feature of porous granular materials: *The lengths that characterize the largest regions of the pore space (the nodes) determine the porosity while those that characterize smallest regions (the throats) determine the*

conductivity. These two lengths vary differently as the system evolves toward lower porosity and thus the relation between σ and ϕ is nontrivial. (This point is also made in Ref. 5; it is gratifying to see the same ideas emerge from what might appear to be two very different models.)

III. DENSE RANDOM PACKING

A. Geometrical considerations

The calculations described above will now be extended to systems with irregularly spaced grains. To model the disordered geometry of a sedimentary composite, we choose to use the Bernal distribution,[17,18] i.e., the coordinates of a dense random packing of identical spheres, for the locations of the particle centers. As before, the radii of the particles are allowed to increase in unison and the material's porosity and resistivity are computed as a function of the radius.

It is useful to compare our computations with those recently described by Elam *et al.*,[19] where a similar sphere-growing algorithm was applied, but random numbers were used to generate a Poisson distribution of grain-center coordinates. Beginning with $R=0$, the sphere radii were increased and the system eventually reached a percolation threshold at $\phi_c=0.032\pm0.004$. The central issue in Ref. 19 was to confirm the universality of the critical exponents ν and β by studying the percolation transition in a structurally disordered system. By contrast, our emphasis is on making a realistic model of the behavior of a sedimentary material over a wide range of porosities. The Poisson distribution employed in Ref. 19 is not suitable for this purpose because it does not correspond to a situation in which the original grain-size distribution is at all uniform.[16] Indeed, in the Poisson model neighboring spheres begin to overlap as soon as $R>0$. While some of our results are surprisingly similar to those obtained in Ref. 19, it will be seen that there are important differences in the pore-space geometry generated by the Poisson and Bernal distributions.

Bernal coordinates are difficult to generate on a computer,[20] so we used a set of 7934 coordinates measured by Finney from a randomized mass of steel balls. Finney's measurement techniques are described by Bernal *et al.*[21] and the coordinates' statistical properties are analyzed by Alben *et al.*[22] Most of our computations were performed on the central 5453 spheres to avoid edge effects. In Fig. 3 four stages of the grain-evolution process are shown as the radius varies from 1.0 to 1.270 and the porosity ranges from 0.364 to 0.030. In many respects these illustrations are similar in character to several types of sedimentary rocks (Fig. 4).[23]

A particularly attractive feature of the Poisson distribution employed in Ref. 19 is the fact that it leads to a simple analytical function relating the porosity to the grain radius. Unfortunately, there is no corresponding function available in the case of the Bernal packing. Therefore we used a Monte Carlo sampling technique to measure this relationship. One million points were placed at random within the sample space and, for each of these points, the distance l to the nearest particle center was computed. If the distribution of these distances, $f(l)$, is normalized to unity,

$$\int_0^\infty f(l)dl=1\ , \tag{9a}$$

the porosity-versus-radius relationship is

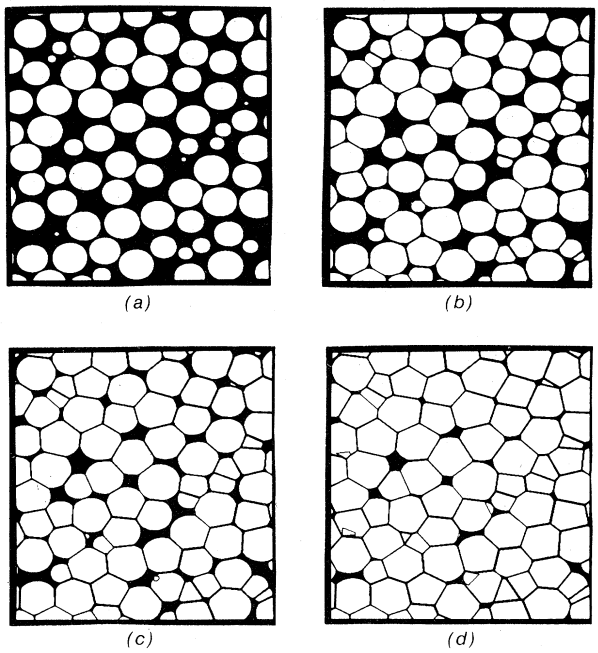

FIG. 3. Computer-synthesized cross sections of a sample of material produced by consolidating a Bernal distribution of spherical grains. The thin lines along the grain-to-grain contacts have been included for clarity and do not represent porosity. The illustrated stages are (a) $\phi=0.364$, the initial configuration, (b) $\phi=0.200$, (c) $\phi=0.100$, where the first occluded volumes have begun to develop, and (d) $\phi=0.030$, near the percolation threshold.

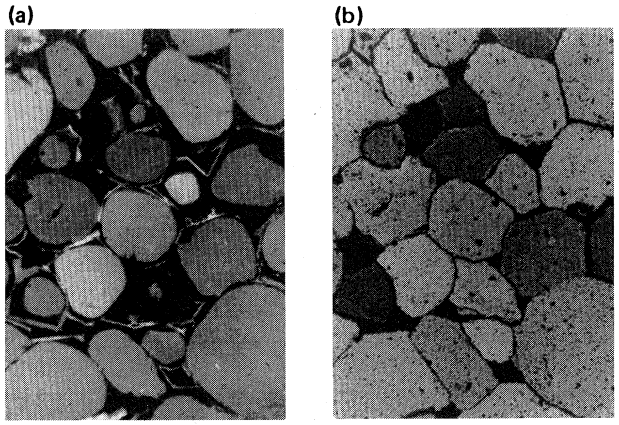

FIG. 4. Heavily cemented Devonian sandstone from Illinois observed (a) with cathodoluminescence to show the original rounded sand grains and (b) with ordinary light to show the angular forms of the grains after cementing. A few small dark pores are visible in (b). [Photos by R. F. Sippel, reproduced courtesy of the American Association of Petroleum Geologists (Ref. 23)].

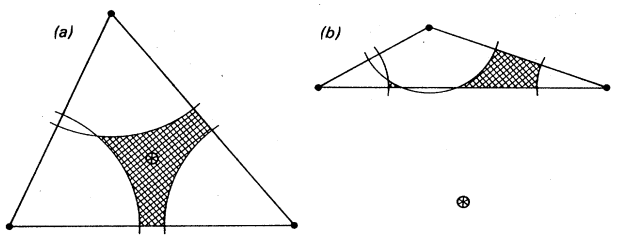

FIG. 5. (a) Typical pore throat (cross-hatched area) produced by three neighboring spheres. In our network analysis the throat is identified with the Voronoi edge (indicated here as a circled sixfold star) running normal to the paper, equidistant from the centers of the three spheres. (b) A distorted pore throat associated with an obtuse triangle of grain centers. Note that the Voronoi edge lies *outside* the triangle. This case is rare when the grains are arranged in a Bernal distribution.

$$\phi(R)=\int_R^\infty f(l)dl \ . \tag{9b}$$

Equation (9b) replaces Eqs. (2)—(4) in the case of ordered packings.

In order to study either electrical conductivity or fluid permeability, it is essential to keep track of the connected paths through the model. To do this, we have followed Kerstein's[24] technique of approximating the continuum problem by a related network problem on the edges and vertices of the Voronoi polyhedra[25] defined by the particle centers. These polyhedra are the analogs of the Wigner-Seitz cells in an ordered packing. Their vertices are equidistant from the four nearest particle centers and may be viewed as the centers of the pore-space nodes described earlier. The edges of the Voronoi polyhedra are equidistant from three particle centers and define the flow paths between the nodes.

Figure 5(a) shows three particles defining a Voronoi edge (which runs normal to the page). This view is taken in the plane of the three particle centers, so it shows the narrowest part of the flow path, i.e., the throat. In Ref. 19 an edge was treated as being "present" if it passed through the pore space when viewed in this plane. We prefer to consider the edge to be present if the triangle among the three particle centers contains a nonzero amount of pore space. This differs from the definition used in Ref. 19 only in the unusual case of obtuse triangles [Fig. 5(b)].

With this definition, our system reached a percolation threshold at $R=1.266$ in the X direction and $R=1.273$ in the Y and Z directions which correspond, respectively, to porosities of $\phi_c=0.032$ and 0.029. (Recall that our calculations are based on a single finite-size system.) These values are remarkably similar to those obtained in the simple and face-centered cubic systems and to those reported in Ref. 19 for the Poisson-generated systems (Table I).

B. Conductivity calculation

Having constructed the model, we next consider the behavior of the electrical conductivity as a function of ϕ. To do this, we make the same assumption as before, namely, that the network's conductivity is controlled by the size of the narrowest parts of the flow channels. For each channel, the throat size can be approximated by the area of the pore space lying in the triangle defined by the three particle centers, as shown by the cross hatching in Fig. 5(a). For various values of R, we computed the sizes of all of the throats and solved the resulting resister network by simple numerical relaxation.[27] Figure 6 shows the computed resistivities, plotted as a function of porosity. This is very similar to the results from the regular lattices shown in Fig. 2. In the disordered medium, the exponent m is equal to approximately 1.80 at high porosities and increases at lower porosities.

Two slight refinements were made on this result. First, the bond conductivities were recalculated by taking the throat area divided by the length of the Voronoi edge. This had very little effect on the results (Fig. 6). Second, we tried to adjust the conductivities to compensate for the funnellike shape of the material's pores. Based on the geometry shown in Fig. 7, a throat with a minimum area equal to πr_0^2 was defined to have an area equal to

$$A(x)=\pi[R+r_0-(R^2-x^2)^{1/2}]^2 \tag{10}$$

on the plane normal to the Voronoi edge at a distance x from the narrowest constriction. The bond's conductivity was then estimated as the harmonic mean:

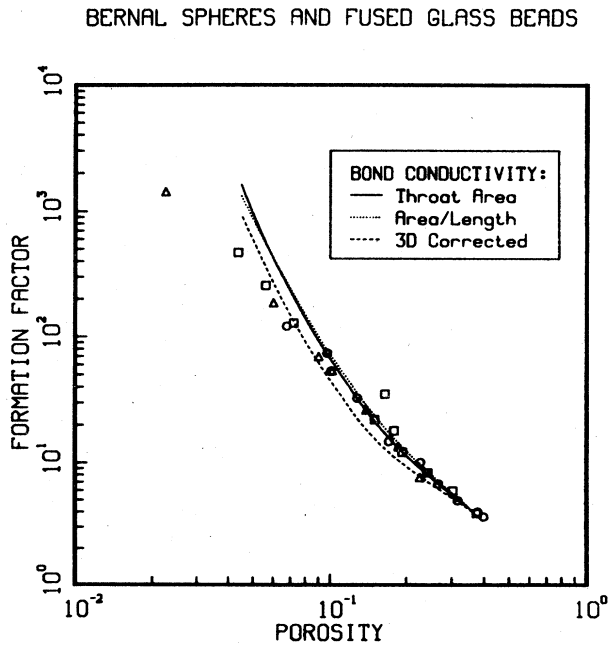

FIG. 6. Estimated formation factor (electrical resistivity) of a disordered aggregate of particles with Bernal-distributed centers. The three curves are computed using different approximations for the conductivity of the individual branches of the pore network (as described in the text). The vertical axis represents the ratio of the bulk resistivity to the fluid resistivity and the symbols represent measurements from three batches of fused glass beads (Ref. 5). A free scaling parameter in the computations has been used to adjust the vertical position of the curves to fit the measurements.

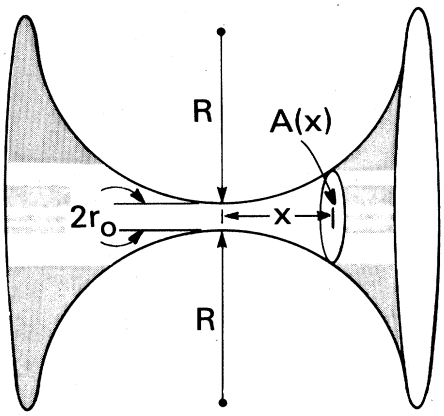

FIG. 7. Funnel-shaped geometry used to approximate the three-dimensional shape of a throat (with minimum cross-sectional area equal to πr_0^2) between two pores.

$$\frac{1}{\sigma_{\text{bond}}} \sim \frac{1}{2R} \int_{-R}^{R} \frac{1}{A(x)} dx \ . \tag{11}$$

These equations can be combined and integrated to give the following form:

$$\frac{1}{\sigma_{\text{bond}}} \sim \frac{2}{\pi} \left[\frac{2}{2Rr_0 + r_0^2} + \frac{4R}{(2Rr_0 + r_0^2)^{3/2}} \tan^{-1}[(2R + r_0)/r_0]^{1/2} \right] . \tag{12}$$

In the limit of very wide channels this equation predicts that the conductivity is, indeed, proportional to the minimum throat area. However, as the channel size (and the material's porosity) decreases, the effective length over which the minimum area is dominant also decreases, and the channel conductivity crosses over the the three-quarters power of the minimum throat area in the limiting case of very narrow channels. This crossover causes some additional curvature in the resistivity plot (Fig. 6) but does not change the curve's essential character.

It should be emphasized that the Bernal-generated model preserves the pore-threat character of the network. Over 97% of the first-neighbor center-to-center distances in the Bernal distribution are between $2R$ and $2\sqrt{2}R$ in length. This guarantees that a great majority of the triangles formed by the centers of three neighboring spheres are acute triangles. Thus, the path followed by the electrical current along the edges of the Voronoi polyhedra almost always lies in well-defined, narrow regions of the kind pictured in Fig. 5(a). By contrast, the Voronoi polyhedra associated with a Poisson distribution of grain centers would lead to a substantial fraction of node-node links governed by obtuse triangles of the kind shown in Fig. 5(b). In this case the arguments we have used to estimate the conductivity are no longer valid and the calculation of σ would be considerably more difficult.

C. Bond statistics

The statistical properties of the bond network in Bernal-generated model deserve further discussion. The percentage of "present" bonds at the percolation threshold was surprisingly high—0.541 for flow in the X direction and 0.523 for flow in the Y or Z directions. By comparison, the diamond lattice has a bond percolation threshold of 0.388 (Ref. 9) and has exactly the same coordination value, 4.0, as the random Voronoi lattice. To convince ourselves that the topological disorder in the present model was *not* responsible for this discrepancy, we tried assigning random numbers (rather than throat areas) to the bonds of the Voronoi lattice. The bonds were then removed in order of the assigned numbers and the system was found to percolate at thresholds ranging from 0.383 to 0.411 in six test cases. These values are sufficiently close to the diamond lattice figure that we have concluded that the high bond percolation thresholds in the original problem were due primarily to correlations among the throat sizes rather than the randomness of the lattice.

Studying this phenomenon further, we created a system with correlated bond values by taking the previous case and averaging each bond's random number with the numbers on all of the adjacent bonds (first neighbors). This caused the percolation threshold to *decrease* rather than increase. In six test cases, the thresholds ranged from 0.241 to 0.286. Finally, we artificially redefined the original problem so that the largest throats would disappear first and the smallest ones would remain to the end. This inverted order gave percolation thresholds of 0.320 in the X and Y directions and 0.321 in the Z direction. These

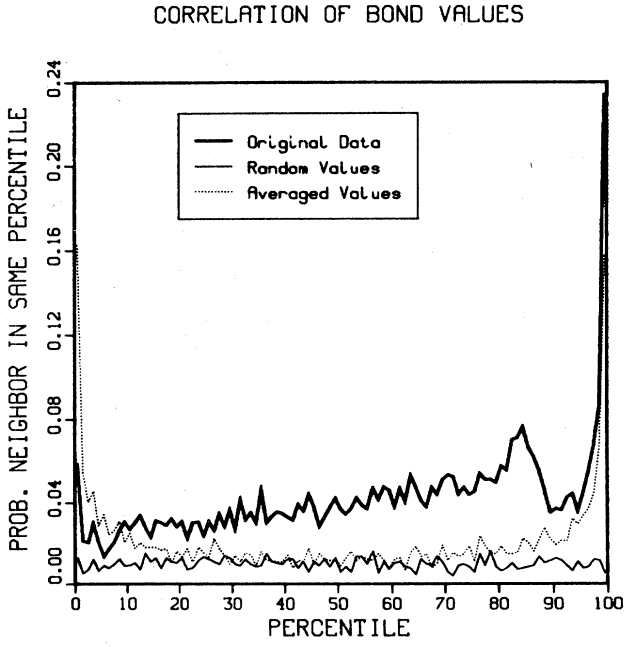

FIG. 8. Bonds on the Voronoi lattice have been grouped into percentiles based on their order of becoming "absent" (i.e., reduced to zero area in the case of pore throats). This plot shows the probability of a bond being in the nth percentile, given that particular one of its neighboring bonds is also in the nth percentile. The three curves represent (1) the Bernal throat data, (2) random bond weights, and (3) random weights which have been averaged with the neighboring bonds' weights.

values, too, are significantly less than in the uncorrelated case.

There seems to be very little published theory to explain this sort of phenomena. Some insight can be gained from Fig. 8, which shows the probability of a bond being in the nth percentile (based on the order of becoming absent), given that a particular one of its immediate neighbors is also in the nth percentile. For the case of randomly assigned bond values, this function is approximately constant at 0.01 (as it should be). When the bond values are averaged with their first neighbors, the function increases slightly in the center and rises very substantially at both ends. The original data has similar peaks at both ends, but has much larger values in the central portion. More importantly, the curve is very asymmetrical. Apparently there is a higher degree of autocorrelation among the more persistent bonds (i.e., the larger throats) than among the others. Physically, this may be due to the presence of clumps of high porosity (such as the larger Bernal holes[17]) in the midst of a relatively homogeneous material of slightly lower porosity. The inverted case (which has a reduced percolation threshold) would represent dense clumps within a homogeneous material of higher porosity. Empirical studies of reservoir rocks[28] indicate that, when samples with the same total porosity are compared, those with isolated dense or open regions are found to have substantially different recovery efficiencies. This may be related to the differences we observe in the percolation threshold for these cases.

IV. CONCLUSIONS

A simple and realistic geometrical model for the consolidation process in sedimentary systems has been developed. This model follows the evolution of the grains from being initially spherical in shape to being more like polyhedra as the material consolidates. Electrical conductivities calculated using this model are consistent with Archie's law over a wide porosity range and are in good agreement with experimental data on fused glass beads.

ACKNOWLEDGMENTS

We are grateful to Po-zen Wong and Joe Tomanic for the use of their experimental data prior to publication and for a series of illuminating discussions regarding its interpretation. G. S. Cargill III provided us with a magnetic tape containing Finney's coordinate data, for which we are very thankful. We have benefited from conversations with William Murphy, Pabitra Sen, Joel Koplik, and Etienne Guyon. We are grateful to J. Banavar for an important suggestion and to B. Halperin and S. Feng for discussions on the behavior of Eq. (12).

---

[1]G. E. Archie, Trans. AIME **146**, 54 (1942).

[2]P. N. Sen, C. Scala, and M. Cohen, Geophysics **46**, 781 (1981).

[3]J. R. Banavar, A. B. Harris, and J. Koplik, Phys. Rev. Lett. **51**, 1115 (1983).

[4]D. Wilkinson, J. Langer, and P. N. Sen, Phys. Rev. B **28**, 1081 (1983).

[5]Po-zen Wong, Joel Koplik, and J. P. Tomanic, Phys. Rev. B **30**, 6606 (1984).

[6]V. Schmidt, D. A. McDonald, and R. L. Platt, Bull. Can. Pet. Geol. **25**, 271 (1977).

[7]R. L. Coble, J. Appl. Phys. **32**, 787 (1961).

[8]Y. Bernabe, W. F. Brace, and B. Evans, Mech. Mater. **1**, 173 (1982).

[9]D. Stauffer, Phys. Rep. **54**, No. 1 (1979).

[10]J. M. Taylor, Am. Assoc. Pet. Geol. Bull. **34**, 701 (1950).

[11]W. D. Lowry, Am. Assoc. Pet. Geol. Bull. **40**, 489 (1956).

[12]E. Pittman, in *Physics and Chemistry of Porous Media (Schlumberger-Doll Research), 1984,* edited by D. L. Johnson and P. N. Sen (AIP, New York, 1984), p. 1.

[13]In Ref. 4, a two-dimensional resistor-capacitor network is employed to represent the interpenetrating pore and grain spaces. When random numbers are used to determine whether a given site will be occupied by a resistor or a capacitor, this model predicts that the dc conductivity vanishes at the conventional percolation threshold $\sigma \sim \sigma_f(\phi - \phi_c)^t$. While the model described in Ref. 4 differs from those developed in Refs. 2, 3, and 5 in this repsect, it has in common with these models the fact that it relies on disorder to obtain a nontrivial power law.

[14]J. E. Owen, Trans. AIME **195**, 169 (1952).

[15]D. L. Johnson, T. J. Plona, F. Pasierb, and H. Kojima, Phys. Rev. Lett. **49**, 1840 (1982).

[16]The sedimentation process by which many sandstones are formed tends to favor distributions of particles that are roughly equal in size (Ref. 12). In this regard, the present algorithm could be contrasted with one in which the porosity is reduced by adding additional spheres with smaller and smaller radii to progressibely fill the pore space of the original packing. To achieve a comparable porosity range by this method, one would have to employ spheres whose radii vary over several orders of magnitude, and the final configuration would bear little resemblance to most naturally occurring porous materials.

[17]J. D. Bernal, Nature (London) **185**, 68 (1960).

[18]J. G. Berryman, Phys. Rev. A **27**, 1053 (1983).

[19]W. T. Elam, A. R. Kerstein, and J. J. Rehr, Phys. Rev. Lett. **52**, 1516 (1984).

[20]D. S. Boudreaux, in *The Magnetic, Chemical and Structural Properties of Glassy Metallic Alloys,* edited by R. Hasegawa (Chemical Rubber, Boca Raton, 1981).

[21]J. D. Bernal, I. A. Cherry, J. L. Finney, and K. R. Knight, J. Phys. E **3**, 388 (1970).

[22]R. Alben, G. S. Cargill III, and J. Wenzel, Phys. Rev. B **13**, 835 (1976).

[23]P. A. Scholle, *A Color Illustrated Guide to Constituents, Textures, Cements and Porosities of Sandstones and Associated Rocks* (American Association of Petroleum Geologists, Tulsa, 1979).

[24]A. Kerstein, J. Phys. A **16**, 3071 (1983).

[25]L. A. Santalo, *Integral Geometry and Geometric Probability* (Addison-Wesley, Reading, 1976).

[26]With only three measurements, 0.032, 0.029, and 0.029, representing the percolation thresholds in the X, Y, and Z

directions through a single finite sample, it is impossible to know the exact size of the statistical and systematic errors. The value given here seems to be a reasonable estimate, given the size of the sample and the consistency of the three measurements.

[27]L. A. Hageman and D. M. Young, *Applied Iterative Methods* (Academic, New York, 1981).

[28]N. C. Wardlaw and J. P. Cassan, Bull. Can. Pet. Geol. **26**, 572 (1978).

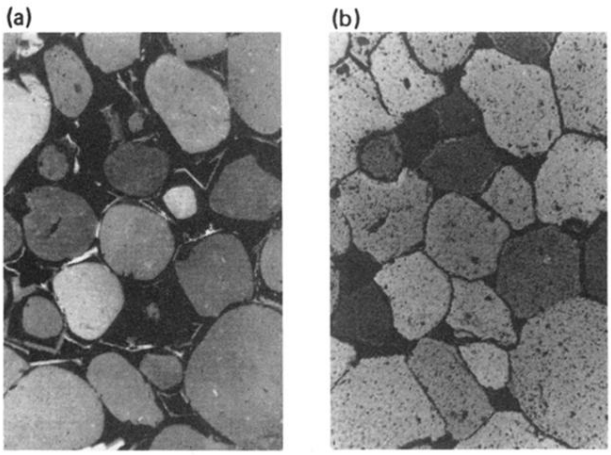

FIG. 4. Heavily cemented Devonian sandstone from Illinois observed (a) with cathodoluminescence to show the original rounded sand grains and (b) with ordinary light to show the angular forms of the grains after cementing. A few small dark pores are visible in (b). [Photos by R. F. Sippel, reproduced courtesy of the American Association of Petroleum Geologists (Ref. 23)].